Journal of Thermal Analysis and Calorimetry (2021) 143:1157–1174
https://doi.org/10.1007/s10973-020-09391-7

Melting heat transfer in squeezing flow of basefluid (water), nanofluid (CNTs + water) and hybrid nanofluid (CNTs + CuO + water)

Khursheed Muhammad[1] · T. Hayat[1,2] · A. Alsaedi[2] · B. Ahmad[2]

Received: 4 November 2019 / Accepted: 24 January 2020 / Published online: 19 February 2020

Abstract

Unsteady squeezed flow of hybrid nanofluid is investigated in this analysis. Comparison of hybrid nanofluid (using CNTs + CuO) and nanofluid (using CNTs) is emphasized. Water is considered as basefluid. Melting effect and viscous dissipation describe heat transfer features. Entropy production and Bejan number are addressed. Relevant flow expressions (PDEs) are transmitted into ODEs through suitable transformations. By means of numerical method (shooting technique with RK-4 algorithm), the obtained ODEs are solved. Comparative study of basefluid (water), hybrid nanofluid (using CNTs + CuO) and nanofluid (using CNTs) is performed for impacts of involved flow parameters on entropy production rate, velocity, Bejan number and temperature. Further comparative analysis of basefluid (water), hybrid nanofluid (using CNTs + CuO) and nanofluid (using CNTs) is done through numerical evaluation of Nusselt number. Velocity of fluid intensifies for larger values of squeezing parameter, nanoparticle volume fraction for single-walled CNTs or multi-walled CNTs, melting parameter and nanoparticle volume fraction for copper oxide in case of both nanofluid and hybrid nanofluid flow. Temperature of fluid enhances with increment in Eckert number while it can be controlled via larger nanoparticle volume fraction for single-walled CNTs or multi-walled CNTs, squeezing parameter, melting parameter and nanoparticle volume fraction for copper oxide. Rate of heat transfer or Nusselt number increases with larger estimation of squeezing parameter, nanoparticle volume fraction for copper oxide, melting parameter and nanoparticle volume fraction for single-walled CNTs or multi-walled CNTs. Entropy production rate is higher for squeezing parameter, melting parameter and Eckert number. Bejan number is reduced with melting parameter while it increases for larger squeezing parameter and Eckert number. During comparative analysis, the performance of hybrid nanofluid is efficient.

Keywords Melting heat · Squeezing flow · Hybrid nanofluid · Entropy production · Numerical solution

List of symbols

u, v	Components of velocity
x, y	Cartesian coordinate system
μ_f	Fluid dynamic viscosity
ν_f	Kinematic fluid viscosity
ρ_f	Fluid density
k_f	Fluid thermal conductivity
α_f	Thermal diffusivity of fluid
f'	Non-dimensional velocity
θ	Non-dimensional temperature
T_f	Temperature of hot fluid
T_m	Melting surface temperature
Ec_x	Local Eckert number
CNTs	Carbon nanotubes
SWCNTs	Single-walled CNTs
$(c_p)_f$	Specific heat of fluid
Pr	Prandtl number
τ_{xy}	Shear stress
ϕ_1	CNTs volume fraction
p	Pressure
Sq	Squeezing parameter
M	Melting parameter
Ec	Eckert number
k_{CNT}	Thermal conductivity of CNTs
k_{CuO}	Thermal conductivity of CuO
MWCNTs	Multiple-walled CNTs
CuO	Copper oxide
ϕ_2	CuO volume fraction

✉ Khursheed Muhammad
kmuhammad@math.qau.edu.pk; khursheedfaiq@gmail.com

1 Department of Mathematics, Quaid-I-Azam University, Islamabad 44000, Pakistan

2 Nonlinear Analysis and Applied Mathematics (NAAM) Research Group, Department of Mathematics, Faculty of Science, King Abdulaziz University, Jeddah, Saudi Arabia

Hybrid Nanofluid

μ_{hnf}	Dynamic viscosity
ν_{hnf}	Kinematic viscosity
ρ_{hnf}	Density
k_{hnf}	Thermal conductivity
α_{hnf}	Thermal diffusivity
$(c_{\mathrm{p}})_{\mathrm{hnf}}$	Specific heat

Nanofluid

k_{nf}	Thermal conductivity
α_{nf}	Thermal diffusivity
$(c_{\mathrm{p}})_{\mathrm{nf}}$	Specific heat
μ_{nf}	Dynamic viscosity
ν_{nf}	Kinematic viscosity
ρ_{nf}	Density

Introduction

The dispersion of nanoparticles in the basefluid is modern way to increase its heat transportation performance. Basefluids include organic liquid, oils, polymer solution, water, biofluids, etc., while nanoparticles are made from metallic oxides (Al_2O_3, CuO, TiO_2, ZnO), metals (Ag, Au, Cu), nitrate ceramics (AIN, TiC, SIC), carbides and CNTs (carbon nanotubes). Nanoparticles comprise size from 1 to 100 nm. The mixture or combination of basefluid and nanoparticles is referred as nanofluid. Thermal features of basefluid can be highly affected by submersion of nanoparticles. Initial step in this domain was taken by Choi [1]. Nanofluids have vital applications in solar cells, drug delivery systems, computer devices, refrigerants, solar collectors, solar thermoelectric devises, cooling and heating of modern systems, etc. Radiation impact in melting flow of CNTs with chemical reactions is explored by Hayat et al. [2]. Hosseini et al. [3] studied heat source, magnetic effect and entropy production in flow of nanofluid. Melting effect in flow of CNTs by numerical approach is presented by Hayat et al. [4]. Entropy production in flow of non-Newtonian fluid is elaborated by Khan et al. [5]. Nanofluid (Cu + water) flow by a down-point rotating cone is presented by Dinarvand and Pop [6]. Hayat et al. [7] examined nanofluid during peristaltic flow with temperature-dependent viscosity. Convective flow of Jeffrey nanofluid between two infinite parallel plates is elaborated by Hayat et al. [8]. Some relevant analysis in this domain can be seen in Refs. [9–19].

Recently, scientists and engineers have performed various experiments on submersion of two or more nanosized particles in same basefluid. Such mixture or combination of nanoparticles and baseliquid is known by hybrid nanofluid. Hybrid nanofluid has exceptional characteristics as compared to nanofluid. A brief study on hybrid nanomaterial is presented by Sarkar et al. [20]. Sajid and Ali [21] analyzed thermal conductance of hybrid nanomaterial. In order to study features of elliptical tube via hybrid nanomaterial, a numerical investigation is given by Huminic and Huminic [22]. Hayat and Nadeem [23] studied heat transport feature via hybrid nanofluid. An experimental analysis on hybrid nanomaterial is performed by Sun et al. [24]. Muhammad et al. [25] performed a comparative analysis of hybrid nanofluid, basefluid and nanofluid in the presence of stagnation point.

Nowadays squeezed flow comprising between two parallel plates is an area of great attention for the scientists and engineers. Squeezed flow is generated due to the motion of the plates toward each other. Applications of squeezed flow in industrial as well as engineering fields include lubrications, metal molding, polymer processing, injection modeling, compression, food processing, etc. Initial analysis in this direction is made by Stefan [26]. Melting impact in rotatory squeezing flow of CNTs is expressed by Hayat et al. [27]. Singeetham and Puttanna [28] elaborated squeezed flow of a non-Newtonian fluid. Slip condition in squeezed flow with double stratification is analyzed by Ahmed et al. [29]. Few recent articles on the topic can be studied in Refs. [30–33].

Existing information on the topic witnessed that very little analysis is yet made about flow of hybrid nanofluid between two parallel plates. Motivation behind this work is to elaborate entropy production in squeezed flow of hybrid nanomaterial. CNTs (SWCNTs, MWCNTs) and CuO are utilized as nanoparticles in water-basefluid. Heat transportation features are explored via viscous dissipation and melting effect. Shooting method (bvp4c) is implemented for solution development. Comparative study for basefluid (water), nanofluid (CNTs (SWCNTs, MWCNTs) + water) and hybrid nanofluid (CNTs (SWCNTs, MWCNTs) + CuO + water) is performed by graphical method.

Formulations

Assume unsteady squeezed flow of hybrid nanofluid bounded between two parallel plates such that the upper plate moves toward the lower fixed plate. The upper plate lies at $y = h(t) = \sqrt{\frac{\upsilon_{\mathrm{f}}(1-bt)}{a}}$ while the lower plate at $y = 0$. Both plates are separated by a distance $h(t) = \sqrt{\frac{\upsilon_{\mathrm{f}}(1-bt)}{a}}$. CNTs and CuO are treated as first and second nanoparticles, respectively, while water is taken as basefluid. In Cartesian coordinates, flow is along x-axis. Here y-axis is perpendicular to the x-axis (see Fig. 1). Flow field expressions under mentioned assumptions are:

$$\frac{\partial u}{\partial x} + \frac{\partial v}{\partial y} = 0, \tag{1}$$

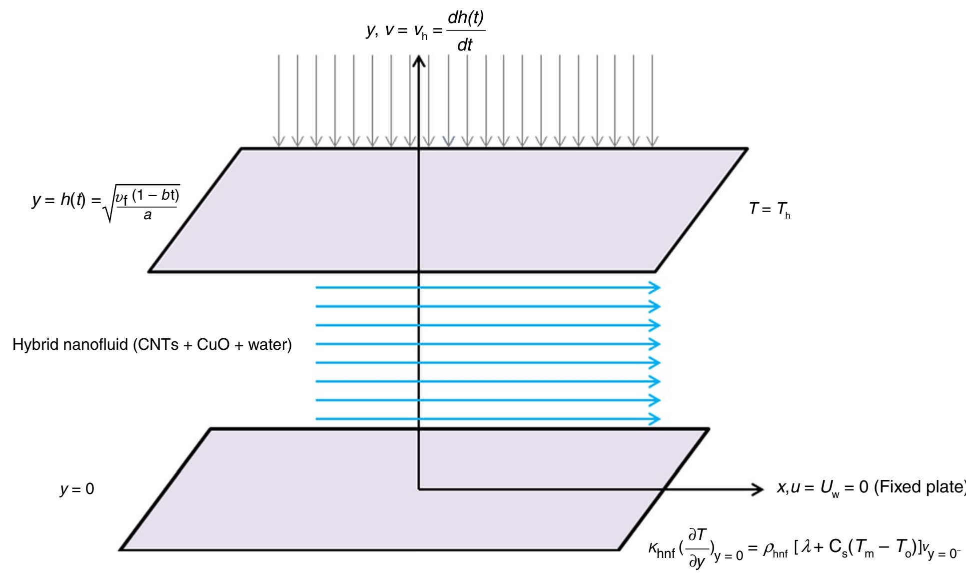

Fig. 1 Schematic diagram for the squeezed flow

$$\frac{\partial u}{\partial t}+u\frac{\partial u}{\partial x}+v\frac{\partial u}{\partial y}=-\frac{1}{\rho_{\mathrm{hnf}}}\frac{\partial p}{\partial x}+\upsilon_{\mathrm{hnf}}\left(\frac{\partial^2 u}{\partial x^2}+\frac{\partial^2 u}{\partial y^2}\right), \tag{2}$$

$$\frac{\partial v}{\partial t}+u\frac{\partial v}{\partial x}+v\frac{\partial v}{\partial y}=-\frac{1}{\rho_{\mathrm{hnf}}}\frac{\partial p}{\partial y}+\upsilon_{\mathrm{hnf}}\left(\frac{\partial^2 v}{\partial x^2}+\frac{\partial^2 v}{\partial y^2}\right), \tag{3}$$

$$\frac{\partial T}{\partial t}+u\frac{\partial T}{\partial x}+v\frac{\partial T}{\partial y}=\alpha_{\mathrm{hnf}}\left(\frac{\partial^2 T}{\partial x^2}+\frac{\partial^2 T}{\partial y^2}\right)+\frac{\mu_{\mathrm{hnf}}}{(\rho c_{\mathrm{p}})_{\mathrm{hnf}}}\left(\frac{\partial u}{\partial y}+\frac{\partial v}{\partial x}\right)^2+\frac{\mu_{\mathrm{hnf}}}{(\rho c_{\mathrm{p}})_{\mathrm{hnf}}}4\left(\frac{\partial u}{\partial x}\right)^2. \tag{4}$$

$$\begin{aligned}&u(x,y,t)=U_{\mathrm{w}}(x,t)=0, T=T_{\mathrm{m}}\text{ at }y=0\\&u(x,y,t)=0, v(x,y,t)=\frac{\mathrm{d}h(t)}{\mathrm{d}t}, T=T_{\mathrm{h}}\text{ at }y=h(t).\end{aligned} \tag{5}$$

Melting condition is [34]:

$$k_{\mathrm{hnf}}\left(\frac{\partial T}{\partial y}\right)=\rho_{\mathrm{hnf}}(\lambda_1+C_s(T_{\mathrm{m}}-T_0))v\text{ at }y=0. \tag{6}$$

Pressure gradient is eliminated from Eqs. (1) and (2) by differentiating Eq. (1) w.r.t y and Eq. (2) w.r.t x.

We consider the transformations for converting the above expressions (PDEs) into ODEs [34]:

$$\eta=\frac{y}{h(t)}, h(t)=\sqrt{\frac{\upsilon_{\mathrm{f}}(1-bt)}{a}}, u=\frac{axf'(\eta)}{1-bt}, v=-\sqrt{\frac{\upsilon_{\mathrm{f}}a}{1-bt}}f(\eta), \theta=\frac{T-T_{\mathrm{m}}}{T_{\mathrm{f}}-T_{\mathrm{m}}}. \tag{7}$$

Condition for incompressibility is verified while other expressions become

$$\frac{A_{11}}{(1-\phi_1)^{2.5}(1-\phi_2)^{2.5}}f^{(\mathrm{iv})}+ff'''-f'f''-\frac{3}{2}\mathrm{Sq}f''-\frac{\mathrm{Sq}}{2}\eta f'''=0, \tag{8}$$

$$\frac{\kappa_{\mathrm{hnf}}}{\kappa_{\mathrm{f}}}\theta''+B_{11}\left(\mathrm{Pr}\,\mathrm{Sq}\left(f\theta'-\frac{\mathrm{Sq}}{2}\eta\theta'\right)\right)+\frac{\mathrm{Pr}}{(1-\phi_1)^{2.5}(1-\phi_2)^{2.5}}(\mathrm{Ec}_x(f'')^2+4\mathrm{Ec}(f')^2))=0, \tag{9}$$

$$f'(0)=0, \theta(0)=0, f(1)=\frac{\mathrm{Sq}}{2}, f'(1)=0, \theta(1)=1, \frac{\kappa_{\mathrm{hnf}}}{\kappa_{\mathrm{f}}}M\theta'(0)+\frac{\mathrm{Pr}}{A_{11}}f(0)=0. \tag{10}$$

Here

$$A_{11}=\frac{1}{(1-\phi_2)\left((1-\phi_1)+\phi_1\frac{\rho_{\mathrm{CNT}}}{\rho_{\mathrm{f}}}\right)+\phi_2\frac{\rho_{\mathrm{CuO}}}{\rho_{\mathrm{f}}}}, \tag{11}$$

$$B_{11}=(1-\phi_2)\left((1-\phi_1)+\phi_1\frac{(\rho c_{\mathrm{p}})_{\mathrm{CNT}}}{(\rho c_{\mathrm{p}})_{\mathrm{f}}}\right)+\phi_2\frac{(\rho c_{\mathrm{p}})_{\mathrm{CuO}}}{(\rho c_{\mathrm{p}})_{\mathrm{f}}}. \tag{12}$$

Associated physical parameters are defined by

$$\mathrm{Sq}=\frac{b}{a}, M=\frac{C_{\mathrm{pf}}(T_\infty-T_{\mathrm{m}})}{\lambda_1+C_{\mathrm{s}}(T_{\mathrm{m}}-T_0)}, \mathrm{Ec}_{\mathrm{x}}=\frac{a^2x^2}{c_{\mathrm{pf}}(T_{\mathrm{f}}-T_{\mathrm{m}})(1-bt)^2}, \mathrm{Pr}=\frac{\nu_{\mathrm{f}}}{\alpha_{\mathrm{f}}}, \mathrm{Ec}=\frac{a\upsilon_{\mathrm{f}}}{c_{\mathrm{pf}}(T_{\mathrm{f}}-T_{\mathrm{m}})(1-bt)}, \Omega=\frac{T_{\mathrm{f}}-T_{\mathrm{m}}}{T_{\mathrm{h}}}. \tag{13}$$

Nusselt number $\left(\mathrm{Nu_x}(Re_x)^{-\frac{1}{2}}\right)$ expression

In dimensional and dimensionless form of $\left(\mathrm{Nu_x}(Re_x)^{-\frac{1}{2}}\right)$ is

$$\mathrm{Nu_x} = \frac{xq_w}{k(T_f - T_h)}, \text{ with } q_w = -k_{hnf}\left(\frac{\partial T}{\partial y}\right)_{y=0,} \tag{14}$$

and

$$\mathrm{Nu_x}(Re_x)^{-\frac{1}{2}} = -\frac{\kappa_{hnf}}{\kappa_f}\theta'(0), \tag{15}$$

where $Re_x = \sqrt{\frac{(1-ct)\upsilon_f}{a}}$ is local Reynolds number.

Entropy production rate (Ns) and Bejan number (Be) expressions

Total entropy production rate (SG_T) is

$$\begin{aligned} SG_T = {} & SG_H(\text{Entropy production through heat transfer}) \\ & + SG_F(\text{Entropy production through fluid friction}). \end{aligned}$$

Thus, we have

$$\begin{aligned} SG_T = {} & \frac{\kappa_{hnf}}{T_h^2}\left(\left(\frac{\partial T}{\partial x}\right)^2 + \left(\frac{\partial T}{\partial y}\right)^2\right) \\ & + \frac{\mu_{nf}}{T_h}\left(4\left(\frac{\partial u}{\partial x}\right)^2 + \left(\frac{\partial v}{\partial x} + \frac{\partial u}{\partial y}\right)^2\right). \end{aligned} \tag{16}$$

In non-dimensional form, entropy production rate (Ns) is

$$\mathrm{Ns} = \frac{SG_T}{SG_0} = \theta'^2 + \frac{\Pr}{\Omega\left(\frac{\kappa_{hnf}}{\kappa_f}\right)(1-\phi_1)^{2.5}(1-\phi_2)^{2.5}}\left(4\mathrm{Ec}f'^2 + \mathrm{Ec}_1 f''^2\right), \tag{17}$$

where SG_0 represents rate of characteristic entropy production and defined by

$$S_{G_0} = \frac{\kappa_{hnf}(T_m - T_h)}{T_h^2 h^2}. \tag{18}$$

Bejan number (Be) is

$$\mathrm{Be} = \frac{SG_H}{SG_T} \tag{19}$$

while Be in dimensionless form is

$$\mathrm{Be} = \frac{\theta'^2}{\mathrm{Ns}}. \tag{20}$$

Model for nanofluid

Expressions for hybrid nanofluid using Hamilton–Crosser model are [12]:

$$\begin{aligned} &\rho_{hnf} = (1-\phi_2)\left((1-\phi_1)\rho_f + \phi_1\rho_{CNT}\right) + \phi_2\rho_{CuO}, \\ &(\rho c_p)_{hnf} = (1-\phi_2)\left((1-\phi_1)(\rho c_p)_f + \phi_1(\rho c_p)_{CNT}\right) + \phi_{2(\rho c_p)CuO}, \\ &\frac{\kappa_{hnf}}{\kappa_{nf}} = \frac{\kappa_{CuO} + (n-1)\kappa_{nf} - (n-1)\phi_2(\kappa_{nf} - \kappa_{CuO})}{\kappa_{CuO} + (n-1)\kappa_{nf} + \phi_2(\kappa_{nf} - \kappa_{CuO})}, \\ &\frac{\kappa_{nf}}{\kappa_f} = \frac{\kappa_{CNT} + (n-1)\kappa_f - (n-1)\phi_1(\kappa_f - \kappa_{CNT})}{\kappa_{CNT} + (n-1)\kappa_f + \phi_1(\kappa_f - \kappa_{CNT})}, \\ &\mu_{hnf} = \frac{\mu_f}{(1-\phi_1)^{2.5}(1-\phi_2)^{2.5}}, \upsilon_{hnf} = \frac{\mu_{hnf}}{\rho_{hnf}}. \end{aligned}$$

For nanofluid, the Hamilton–Crosser expressions are

$$\begin{aligned} &\rho_{nf} = (1-\phi_1)\rho_f + \phi_1\rho_{CNT}, \\ &(\rho c_p)_{nf} = (1-\phi_1)(\rho c_p)_f + \phi_1(\rho c_p)_{CNT}, \\ &\frac{\kappa_{nf}}{\kappa_f} = \frac{\kappa_{CNT} + (n-1)\kappa_f - (n-1)\phi_1(\kappa_f - \kappa_{CNT})}{\kappa_{CNT} + (n-1)\kappa_f + \phi_1(\kappa_f - \kappa_{CNT})}, \\ &\mu_{nf} = \frac{\mu_f}{(1-\phi_1)^{2.5}}, \upsilon_{nf} = \frac{\mu_{nf}}{\rho_{nf}}. \end{aligned}$$

Here n is shape parameter, i.e., $n = 6$ represents that nanoparticles are of tube like or cylindrical shape (Table 1).

Numerical solution

After implementing transformations given in Eq. (7), the transformed flow field expressions are then solved by shooting method (a numerical technique with RK-4 algorithm).

Table 1 Thermal characteristics of CNTs, CuO and water [28]

Nanoparticles/Thermophysical properties	ρ/kg m^{-3}	c_p/J kg^{-1} K^{-1}	κ/W m^{-1} K^{-1}	Pr
SWCNTs	2600	425	6600	–
CuO	6320	531.80	76.50	–
MWCNTs	1600	796	3000	–
Water	997.1	4179	0.613	6.7

Shooting technique with RK-4 is applied only for IBVPs of first order, thus reducing the flow expression into first order as [14]:

$$
\begin{aligned}
&f_{11}=f, f_{12}=f_{11}'=f', f_{13}=f_{12}'=f'', f_{14}=f_{13}'=f''',\\
&f_{21}=\theta, f_{22}=f_{21}'=\theta', f_1=f_{14}'=f^{(iv)}=-A_{11}\left(1-\phi_1\right)^{2.5}\\
&\quad\times\left(1-\phi_2\right)^{2.5}\left(f_{11}f_{14}-f_{12}f_{13}-\frac{3}{2}\mathrm{Sq}f_{13}-\frac{\mathrm{Sq}}{2}\eta f_{14}\right),\\
&f_2=f_{22}''=\theta''=-\frac{B_{11}}{\frac{k_{\mathrm{hnf}}}{k_{\mathrm{f}}}}\left(\Pr Sq(f_{11}f_{22}-\frac{Sq}{2}\eta f_{22}\right)\\
&\quad+\frac{\Pr}{\left(1-\phi_1\right)^{2.5}\left(1-\phi_2\right)^{2.5}}(\mathrm{Ec_x}f_{13}^2+4\mathrm{Ec}f_{12}^2)),\\
&f_{12}(0)=0, f_{21}(0)=0, \frac{k_{\mathrm{hnf}}}{k_{\mathrm{f}}}f_{22}(0)+\frac{\Pr}{\mathrm{MA}_{11}}f_{11}(0)=0,\\
&f_{13}(0)=0, f_2(0)=1, f_{14}(0)=0.
\end{aligned}
$$

Analysis

The vital theme behind this section is to visualize comparative study among basefluid (water), nanofluid (CNTs (water)) and hybrid nanofluid (CNTs + CuO (water)). Velocity of fluid ($f'(\eta)$), rate of entropy production (Ns), temperature of fluid ($\theta(\eta)$) and Bejan number (Be) are studied against higher estimations of Sq, ϕ_1, ϕ_2, M and Ec in Figs. 2a–4r). The graphical visualization is performed as follows:

1. First graph is plotted for comparative analysis of nanofluid (using SWCNTs + water) and hybrid nanofluid (using SWCNTs + CuO + water) against each physical parameter.
2. Second graph is plotted for comparative study of nanofluid and hybrid nanofluid by replacing SWCNTs by MWCNTs.
3. In third graph, the comparative study among nanofluid (using CNTs (SWCNTs, MWCNTs) + water), hybrid nanofluid (using CNTs (SWCNTs, MWCNTs) + CuO + water) and basefluid (using water) is visualized against each pertinent parameter. Here we take $\mathrm{Sq}=M=0.1, \phi_1=\phi_2=0.5, \mathrm{Ec}=\mathrm{Ec_x}=0.5$.

Analysis of velocity ($f'(\eta)$)

In Fig. 2a and b, the variations in $f'(\eta)$ during comparative study of nanofluid (SWCNTs + water, MWCNTs + water) and hybrid nanofluid (SWCNTs + CuO + water, using MWCNTs + CuO + water) are sketched against higher estimations of Sq. Clearly, it is detected that $f'(\eta)$ is an increasing function of Sq and impact of hybrid nanofluid is more than nanofluid. Physically, increment in Sq leads to larger squeezing force experienced by fluid particles. Thus, $f'(\eta)$ intensifies. Velocity of fluid ($f'(\eta)$) via ϕ_1 in comparative study of nanofluid (SWCNTs + water, MWCNTs + water) and hybrid nanofluid (SWCNTs + CuO + water, MWCNTs + CuO + water) is labeled in Fig. 2d and e. Increment in $f'(\eta)$ is noticed via higher ϕ_1, and conspicuous impact is detected for hybrid nanofluid. Impact of M on $f'(\eta)$ during flow of nanofluid (using SWCNTs + water, using MWCNTs + water) and hybrid nanofluid (SWCNTs + CuO + water, MWCNTs + CuO + water) is portrayed in Fig. 2g and h. Direct variations in $f'(\eta)$ are seen against higher M, and dominant trend is noticed for hybrid nanofluid. Indeed higher M leads to more convective flow from melting surface toward hot fluid. Hence, $f'(\eta)$ increases. Figure 2j and k shows the impact of ϕ_2 on $f'(\eta)$ during flow of nanofluid (SWCNTs + water, MWCNTs + water) and hybrid nanofluid (SWCNTs + CuO + water, MWCNTs + CuO + water). As expected, no impact on $f'(\eta)$ is seen for higher ϕ_2 during flow of nanofluid while $f'(\eta)$ intensifies during flow of hybrid nanofluid. Impact of hybrid nanofluid is also dominant. Figure 2c, f, i and l is plotted for impact of basefluid (water), nanofluid (CNTs (SWCNTs + water, MWCNTs + water)) and hybrid nanofluid (CNTs (SWCNTs, MWCNTs) + CuO + water) on $f'(\eta)$ when $\mathrm{Sq}=\phi_1=M=\phi_2=0.1$, respectively. It can be seen clearly that hybrid nanofluid shows effective behavior than that of nanofluid as well as basefluid.

Analysis of temperature ($\theta(\eta)$)

Temperature ($\theta(\eta)$) of fluid against Sq during flow of nanofluid (SWCNTs + water, MWCNTs + water) and hybrid nanofluid (SWCNTs + CuO + water, MWCNTs + CuO + water) is presented in Fig. 3a and b. Temperature ($\theta(\eta)$) decay with higher estimations of Sq and behavior of hybrid nanofluid is prominent. Physically, higher Sq leads to stronger squeezing force which results in closeness of both plates. Thus, decay in kinematic velocity leads to reduction in $\theta(\eta)$. Figure 3d and e depicts the impact of ϕ_1 on $\theta(\eta)$ during comparative study of nanofluid (using SWCNTs + water, using MWCNTs + water) and hybrid nanofluid (using SWCNTs + CuO + water, using MWCNTs + CuO + water). $\theta(\eta)$ decays with higher ϕ_1, and hybrid nanofluid shows effective behavior. $\theta(\eta)$ against M is sketched in Fig. 3g and h during comparative study of nanofluid (SWCNTs + water, MWCNTs + water) and hybrid nanofluid

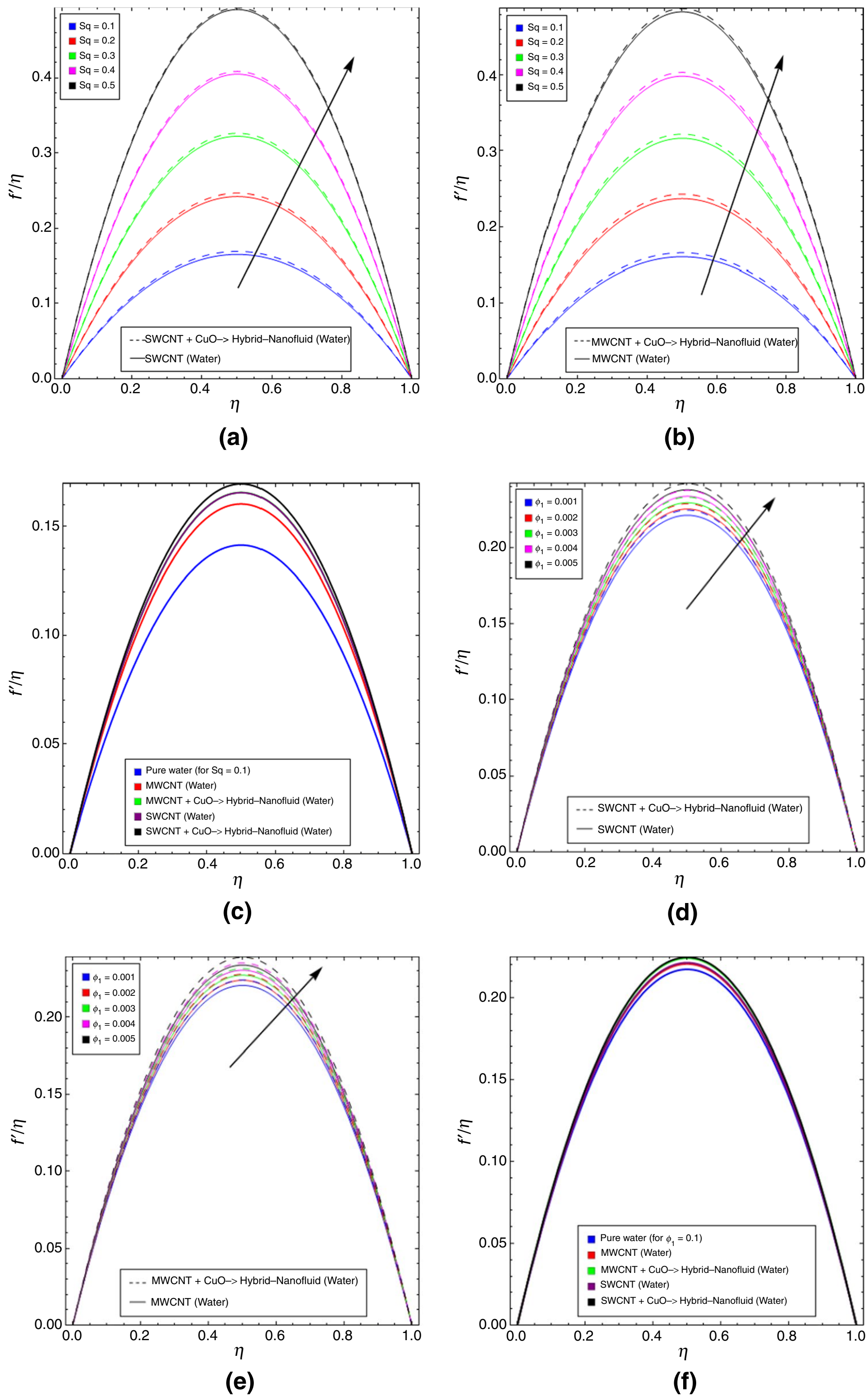

Fig. 2 **a** $f'(\eta)$ vs. Sq (SWCNTs + CuO + water), **b** $f'(\eta)$ vs. Sq (MWCNTs + CuO + water), **c** $f'(\eta)$ vs. Sq (comparison), **d** $f'(\eta)$ vs. ϕ_1 (SWCNTs + CuO + water), **e** $f'(\eta)$ vs. ϕ_1 (MWCNTs + CuO + water), **f** $f'(\eta)$ vs. ϕ_1 (comparison), **g** $f'(\eta)$ vs. M (SWCNTs + CuO + water), **h** $f'(\eta)f'(\eta)$ vs. M (MWCNTs + CuO + water). **i** $f'(\eta)$ vs. M (comparison), **j** $f'(\eta)$ vs. ϕ_2 (SWCNTs + CuO + water), **k** $f'(\eta)$ vs. ϕ_2 (MWCNTs + CuO + water), **l** $f'(\eta)$ vs. ϕ_2 (comparison)

(SWCNTs + CuO + water, MWCNTs + CuO + water). $\theta(\eta)$ reduces with higher M, and behavior of hybrid nanofluid is prominent when compared with nanofluid. Indeed higher M leads to addition of cold fluid particles from melting surface to heated fluid. Thus, $\theta(\eta)$ decays. Figure 3j and k presents impact of ϕ_2 on $\theta(\eta)$ during flow of nanofluid

Fig. 2 (continued)

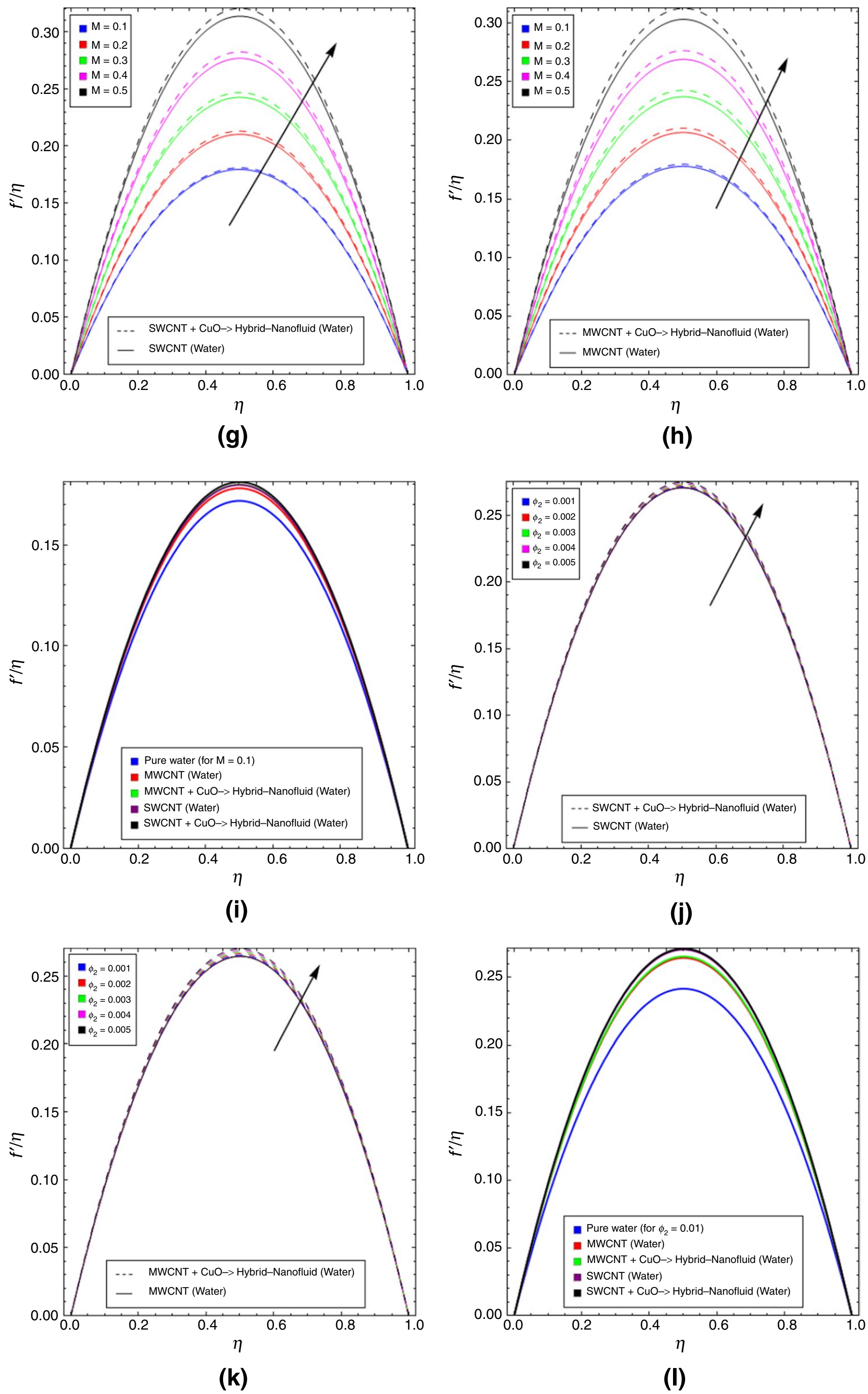

(SWCNTs + water, MWCNTs + water) and hybrid nanofluid (SWCNTs + CuO + water, MWCNTs + CuO + water). Decrease in $\theta(\eta)$ is observed for higher ϕ_2, and clearly, hybrid nanofluid shows effective trend. $\theta(\eta)$ against Ec during flow of nanofluid (SWCNTs + water, MWCNTs + water) and hybrid nanofluid (SWCNTs + CuO + water,

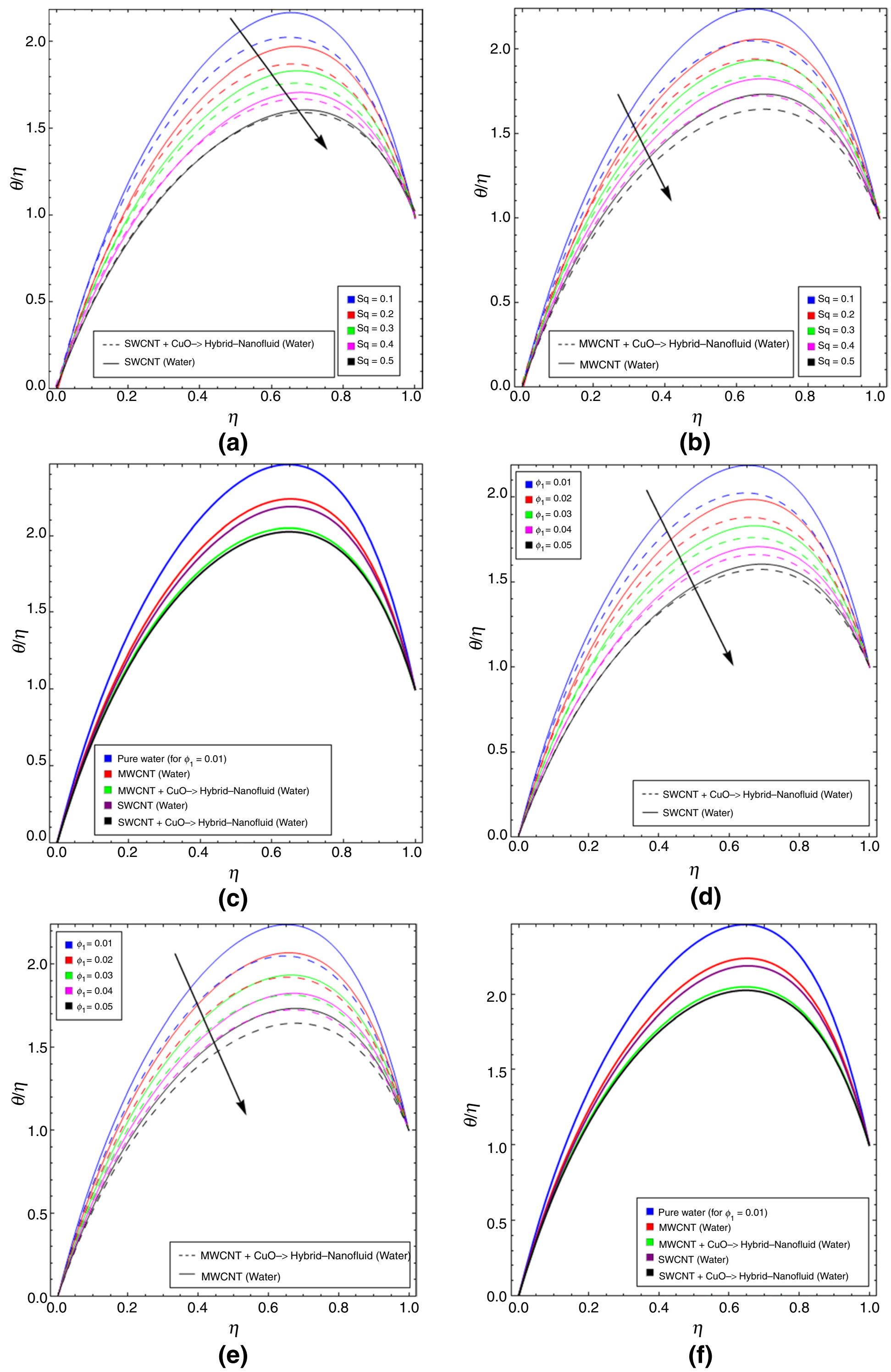

Fig. 3 **a** $\theta(\eta)$ vs. Sq (SWCNTs + CuO + water), **b** $\theta(\eta)$ vs. Sq (MWCNTs + CuO + water), **c** $\theta(\eta)$ vs. Sq (comparison), **d** $\theta(\eta)$ vs. ϕ_1 (SWCNTs + CuO + water), **e** $\theta(\eta)$ vs. ϕ_1 (MWCNTs + CuO + water), **f** $\theta(\eta)$ vs. ϕ_1 (comparison), **g** $\theta(\eta)$ vs. M (SWCNTs + CuO + water), **h** $\theta(\eta)$ vs. M (MWCNTs + CuO + water), **i** $\theta(\eta)$ vs. M (comparison), **j** $\theta(\eta)$ vs. ϕ_2 (SWCNTs + CuO + water), **k** $\theta(\eta)$ vs. ϕ_2 (MWCNTs + CuO + water), **l** $\theta(\eta)$ vs. ϕ_2 (comparison), **m** $\theta(\eta)$ vs. Ec (SWCNTs + CuO + water), **n** $\theta(\eta)$ vs. Ec (MWCNTs + CuO + water), **o** $\theta(\eta)$ vs. Ec (comparison)

MWCNTs + CuO + water) is plotted in Fig. 3m and n. Here $\theta(\eta)$ directly varies with Ec, and hybrid nanofluid shows overriding trend. Physically, higher Ec leads to production of more drag force between fluid particles and so $\theta(\eta)$ intensifies. Figure 3c, f, i, l, o is labeled to examine $\theta(\eta)$ during flow of basefluid (water), nanofluid (using CNTs (SWCNTs, MWCNTs) + water) and hybrid nanofluid (using CNTs (SWCNTs, MWCNTs) + CuO + water) when

Fig. 3 (continued)

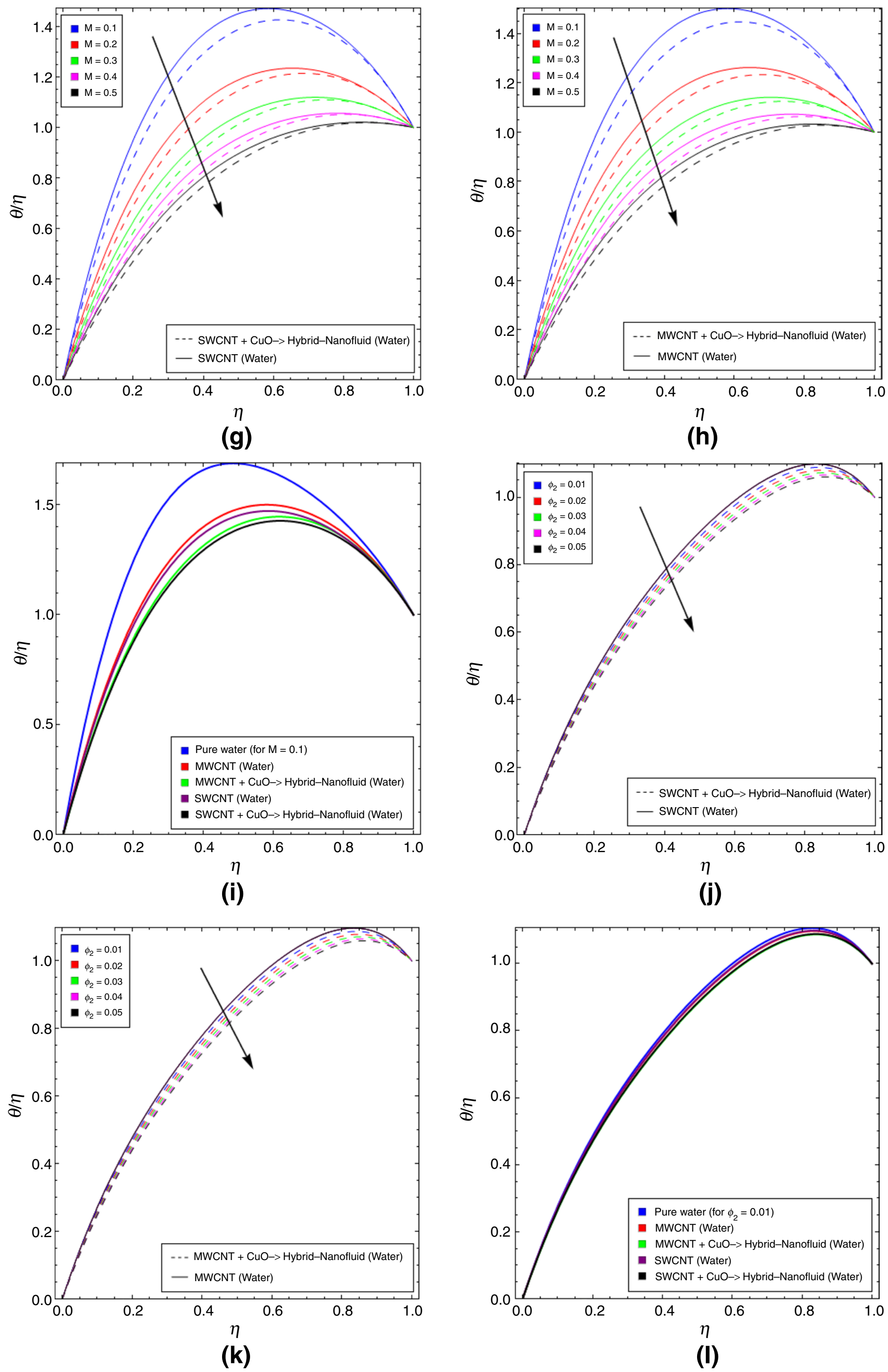

Sq = $\phi_1 = M = \phi_2 =$ Ec = 0.1. As expected, better performance is shown by hybrid nanofluid than nanofluid and basefluid, respectively.

Analysis for rate of entropy production (Ns) and Bejan number (Be)

Entropy production (Ns) against Sq during comparative study of nanofluid (using SWCNTs + water, using MWCNTs + water)

Fig. 3 (continued)

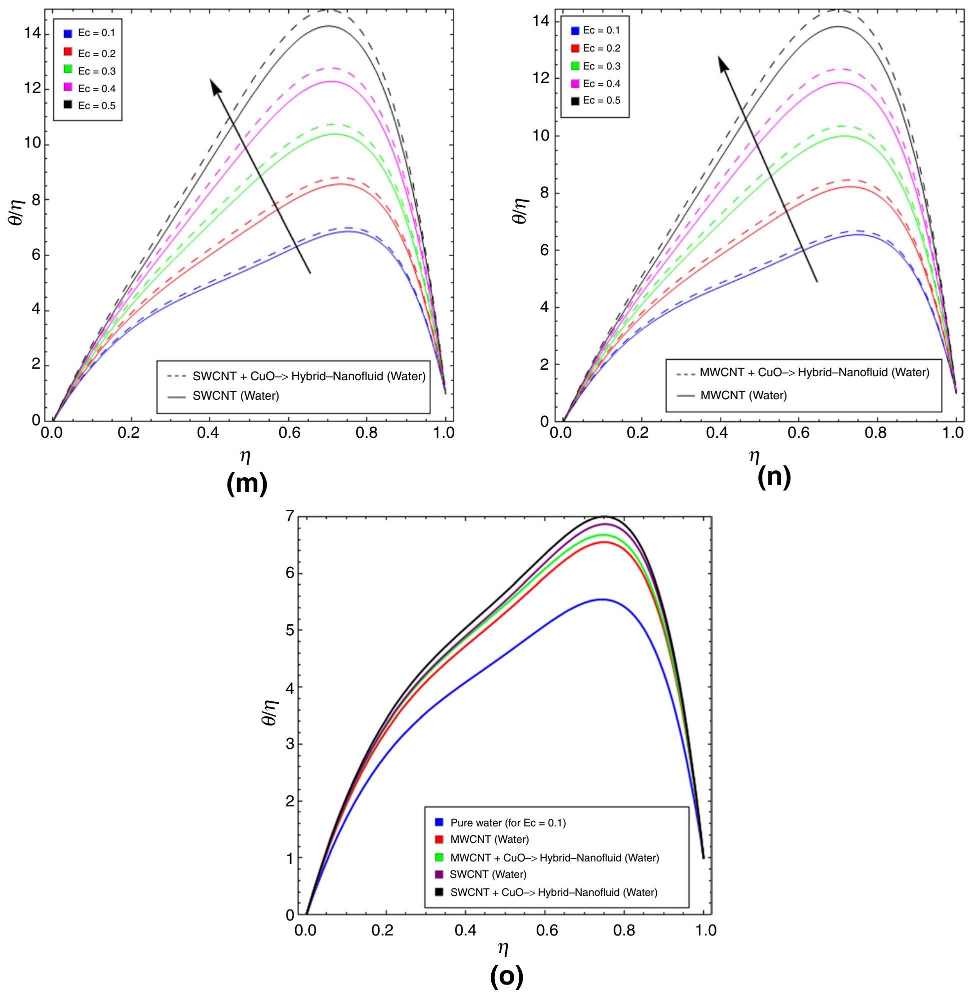

and hybrid nanofluid (SWCNTs + CuO + water, MWCNTs + CuO + water) is depicted in Fig. 4a and b. *Ns* intensifies with higher Sq, and prominent impact is observed for nanofluid. Further entropy production (Ns) is higher at the walls. *Ns* via higher estimations of *M* in comparative analysis of nanofluid (using SWCNTs + water, using MWCNTs + water) and hybrid nanofluid (SWCNTs + CuO + water, MWCNTs + CuO + water) is labeled in Fig. 4d and e. Intensification in *Ns* is observed, and nanofluid shows prominent behavior. Also entropy production (Ns) is larger near the walls. Figure 4g and h is portrayed for *Ns* against Ec during flow of nanofluid (using SWCNTs + water, using MWCNTs + water) and hybrid nanofluid (using SWCNTs + CuO + water, using MWCNTs + CuO + water). Clearly, *Ns* intensifies with larger Ec and impact of nanofluid is dominant. Entropy production *Ns* during comparative study of basefluid (water), nanofluid (using CNTs (SWCNTs, MWCNTs) + water) and hybrid nanofluid (using CNTs (SWCNTs, MWCNTs) + CuO + water) when $\mathrm{Sq} = M = \mathrm{Ec} = 0.1$ is studied in Fig. 4c, f, i, respectively. Impact of nanofluid is dominant which is followed by hybrid nanofluid and basefluid. In order to study comparison between entropy production through heat transfer (N_H) and through fluid friction (N_F), Bejan number (Be) against η is plotted. Be lies in between 0 and 1. N_H dominates over N_F when $\mathrm{Be} \in (0.5,\ 1]$ while N_F dominates over N_H when $\mathrm{Be} \in [0.0.5)$. Be versus higher estimations of Sq during flow of nanofluid (SWCNTs + water, MWCNTs + water) and hybrid nanofluid (SWCNTs + CuO + water, MWCNTs + CuO + water) is presented in Fig. 4j and k. Be intensifies with increment in Sq, and impact of hybrid nanofluid is more than nanofluid. Further, it is clear that N_F is dominant over N_H. Figure 4m and n is labeled for Be against *M* during comparative study between nanofluid (SWCNTs + water, MWCNTs + water) and hybrid nanofluid (SWCNTs + CuO + water, MWCNTs + CuO + water). Decay in

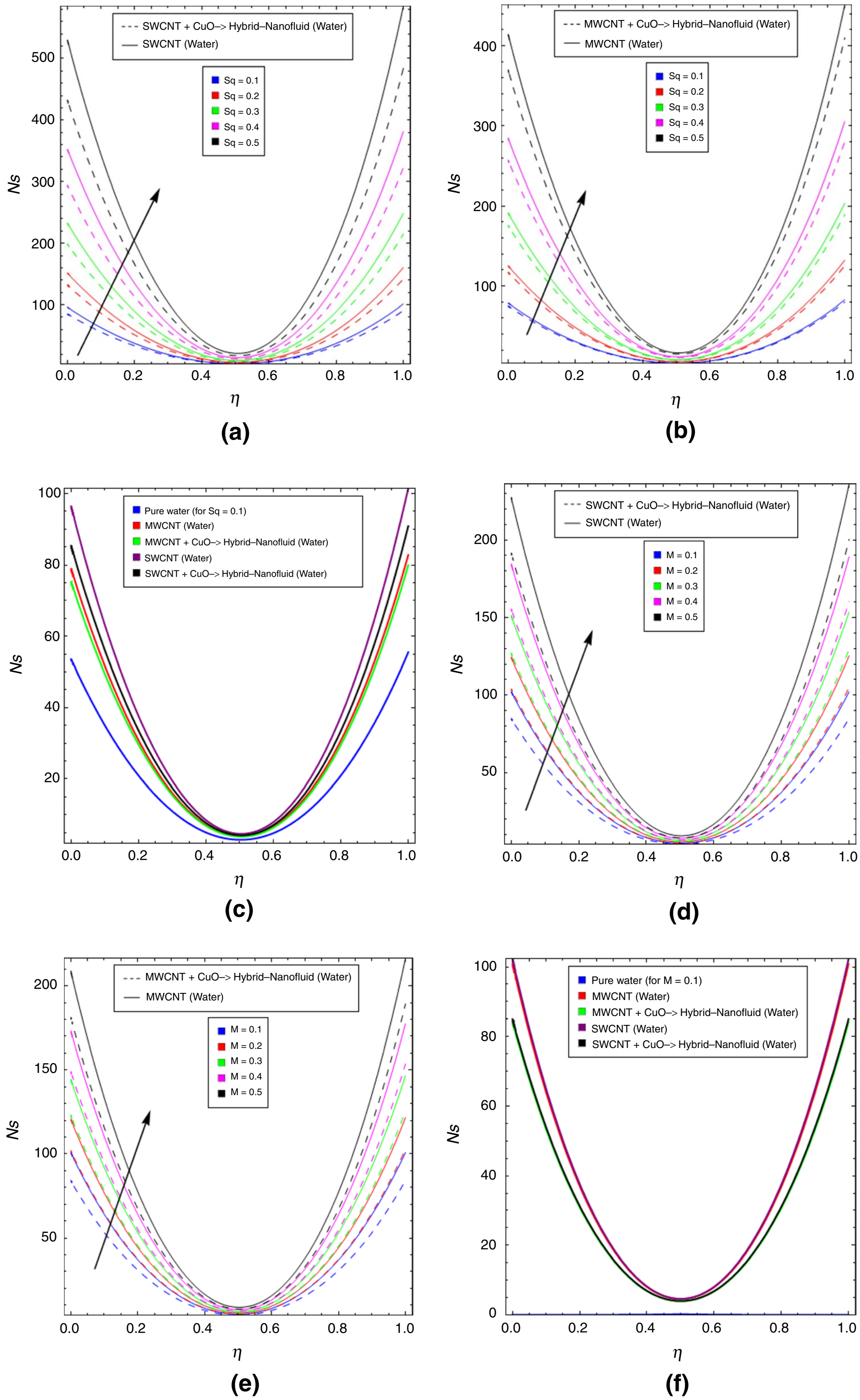

Fig. 4 a Ns vs. Sq (SWCNTs + CuO + water), **b** Ns vs. Sq (MWCNTs + CuO + water), **c** Ns vs. Sq (comparison), **d** Ns vs. Ns (SWCNTs + CuO + water), **e** Ns vs. *M* (MWCNTs + CuO + water), **f** Ns vs. *M* (comparison), **g** Ns vs. Ec (SWCNTs + CuO + water), **h** Ns vs. Ec (MWCNTs + CuO + water), **i** Ns vs. Ec (comparison), **j** Be vs. Sq (SWCNTs + CuO + water), **k** Be vs. Sq (MWCNTs + CuO + water), **l** Be vs. Sq (comparison), **m** Be vs. *M* (SWCNTs + CuO + water), **n** Be vs. *M* (MWCNTs + CuO + water), **o** Be vs. *M* (comparison), **p** Be vs. Ec (SWCNTs + CuO + water), **q** Be vs. Ec (MWCNTs + CuO + water), **r** Be vs. Ec (comparison)

Fig. 4 (continued)

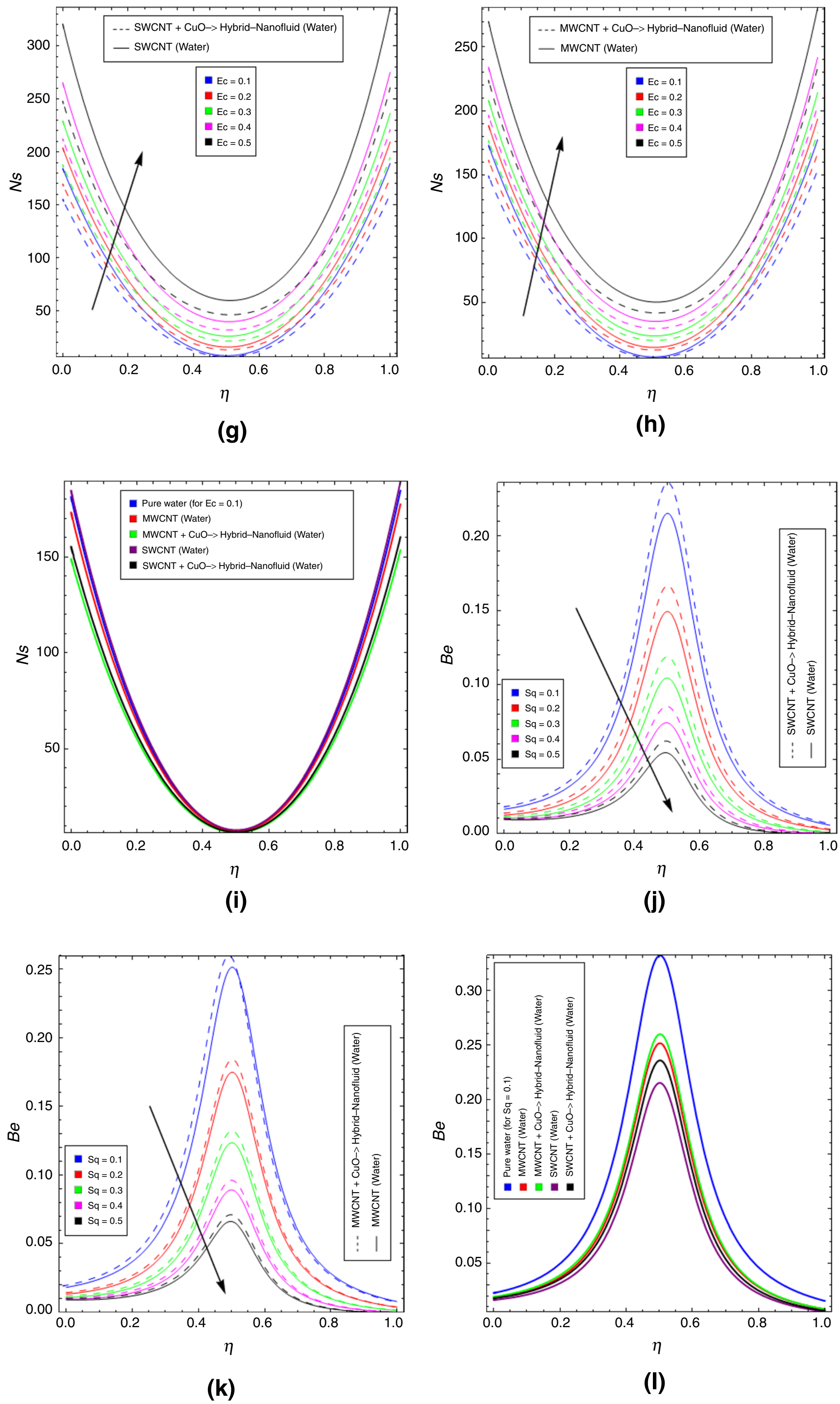

Fig. 4 (continued)

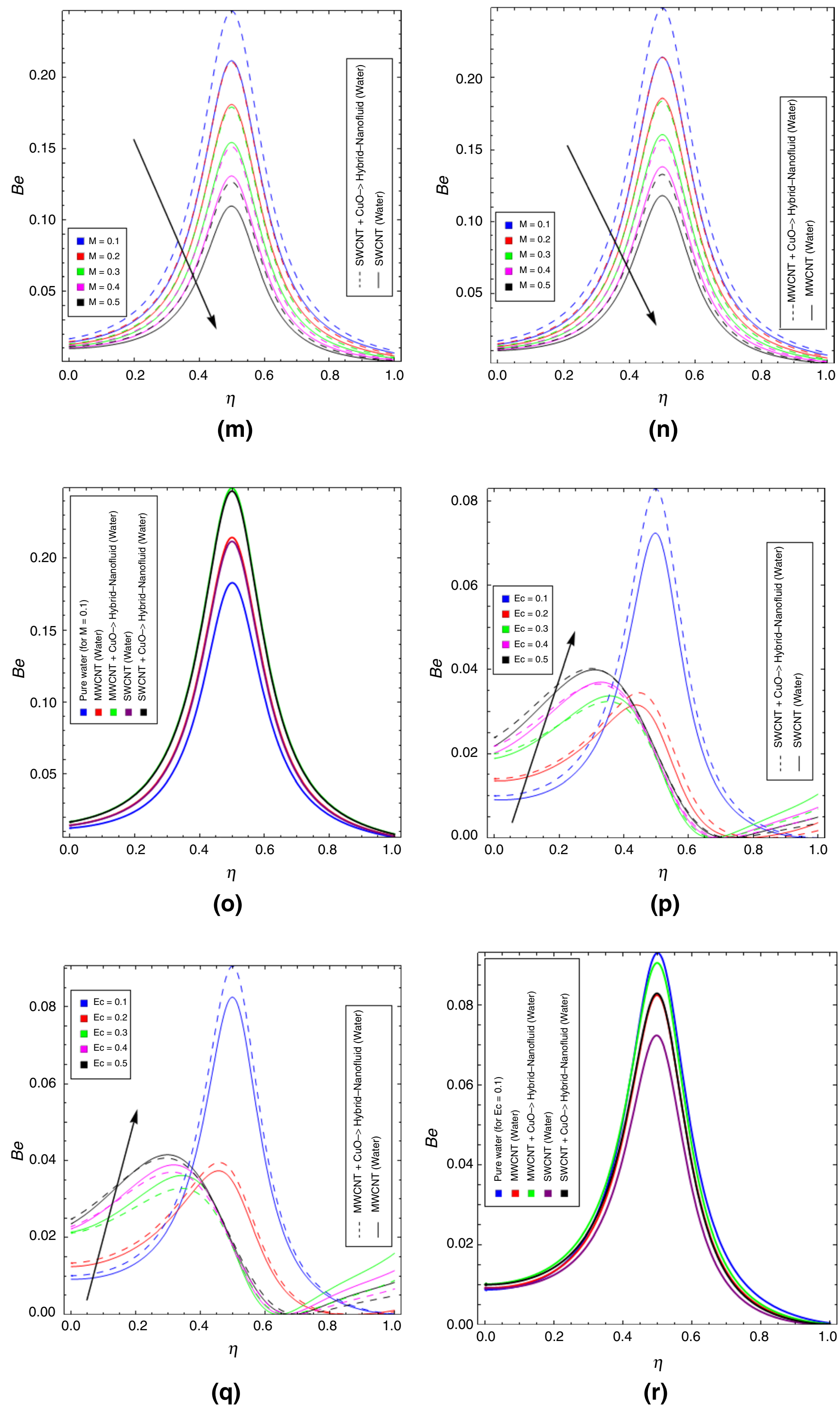

Table 2 Evaluation of Nusselt number $(Nu_x(Re_x)^{-\frac{1}{2}})$ for various estimations of ϕ_1, ϕ_2, M and Sq when $Ec = Ec_x = 0.1$

ϕ_1	ϕ_2	M	Sq	Water	MWCNTs (nanofluid)	MWCNTs + CuO (hybrid nanofluid)	SWCNTs (nanofluid)	SWCNTs + CuO (hybrid nanofluid)
0.01	0.05	0.5	0.5	1.00331	1.0685	1.68929	1.06917	1.68986
0.02				1.00331	1.1352	1.79109	1.13668	1.79239
0.03				1.00331	1.20347	1.89513	1.20593	1.89731
0.04				1.00331	1.27335	2.00146	1.27697	2.00471
0.05				1.00331	1.34491	2.11019	1.34991	2.11471
0.01	0.01	0.4	0.2	1.00331	1.64929	1.74339	1.66229	1.75617
	0.02			1.00331	1.64929	1.83941	1.66229	1.85201
	0.03			1.00331	1.64929	1.9374	1.66229	1.94986
	0.04			1.00331	1.64929	2.03744	1.66229	2.04979
	0.05			1.00331	1.64929	2.1396	1.66229	2.15186
0.01	0.01	0.1	0.2	0.969549	1.57437	2.4564	1.57516	2.45695
		0.2		0.978019	1.59233	2.48384	1.59562	2.48679
		0.3		0.989171	1.61695	2.52147	1.62416	2.52816
		0.4		1.00331	1.64929	2.5709	1.66229	2.58308
		0.5		1.02087	1.691	2.63458	1.71244	2.66231
0.01	0.01	0.4	0.1	1.00331	1.0685	1.13184	1.06917	1.13249
			0.2	1.02677	1.09486	1.16033	1.0958	1.16126
			0.3	1.09232	1.16402	1.23237	1.16535	1.23367
			0.4	1.20068	1.27689	1.34894	1.27871	1.35072
			0.5	1.35178	1.43357	1.5103	1.43602	1.5127

Be is noticed, and nanofluid shows effective trend when compared with hybrid nanofluid. N_F also dominates over N_H. Be via higher estimations of Ec during flow of nanofluid (SWCNTs (water), MWCNTs (water)) and hybrid nanofluid (SWCNTs + CuO + water, MWCNTs + CuO + water) is portrayed in Fig. 4p and q. Increment in Be is detected while hybrid nanofluid shows overriding trend. N_F dominates over N_H. Be during comparative analysis of basefluid (water), nanofluid nanofluid (using CNTs (SWCNTs, MWCNTs) + water) and hybrid nanofluid (using CNTs (SWCNTs, MWCNTs) + CuO + water) when $Sq = M = Ec = 0.1$ is visualized in Fig. 4c, f, i, l, o, r. As expected, better trend is seen for hybrid nanofluid followed by nanofluid and basefluid, respectively.

Analysis of Nusselt number $(Nu_x(Re_x)^{-\frac{1}{2}})$

Nusselt number $(Nu_x(Re_x)^{-\frac{1}{2}})$ against higher estimations of ϕ_1, ϕ_2, M and Sq during flow basefluid (water), nanofluid (using CNTs (SWCNTs, MWCNTs) + water) and hybrid nanofluid (using CNTs (SWCNTs, MWCNTs) + CuO + water) is evaluated in Table 2. It is founded that $Nu_x(Re_x)^{-\frac{1}{2}}$ intensify with higher estimations of mentioned physical parameters. It is analyzed that effect of hybrid nanofluid is efficient which is followed by nanofluid and basefluid, respectively.

Comparison of current analysis with previously published work on nanofluid using Buongiorno model

In this section, we have compared our theoretical analysis on hybrid nanofluid with previously published work on nanfluid by Farooq et al. [35]. Excellent agreements are founded for the covering parameters. Same impacts of Sq and Mon $f'(\eta)$ as well as $\theta(\eta)$ are founded. Similarly, impacts of Sq and Mon Nusselt number in both published and current analysis have a great agreement (Fig. 5).

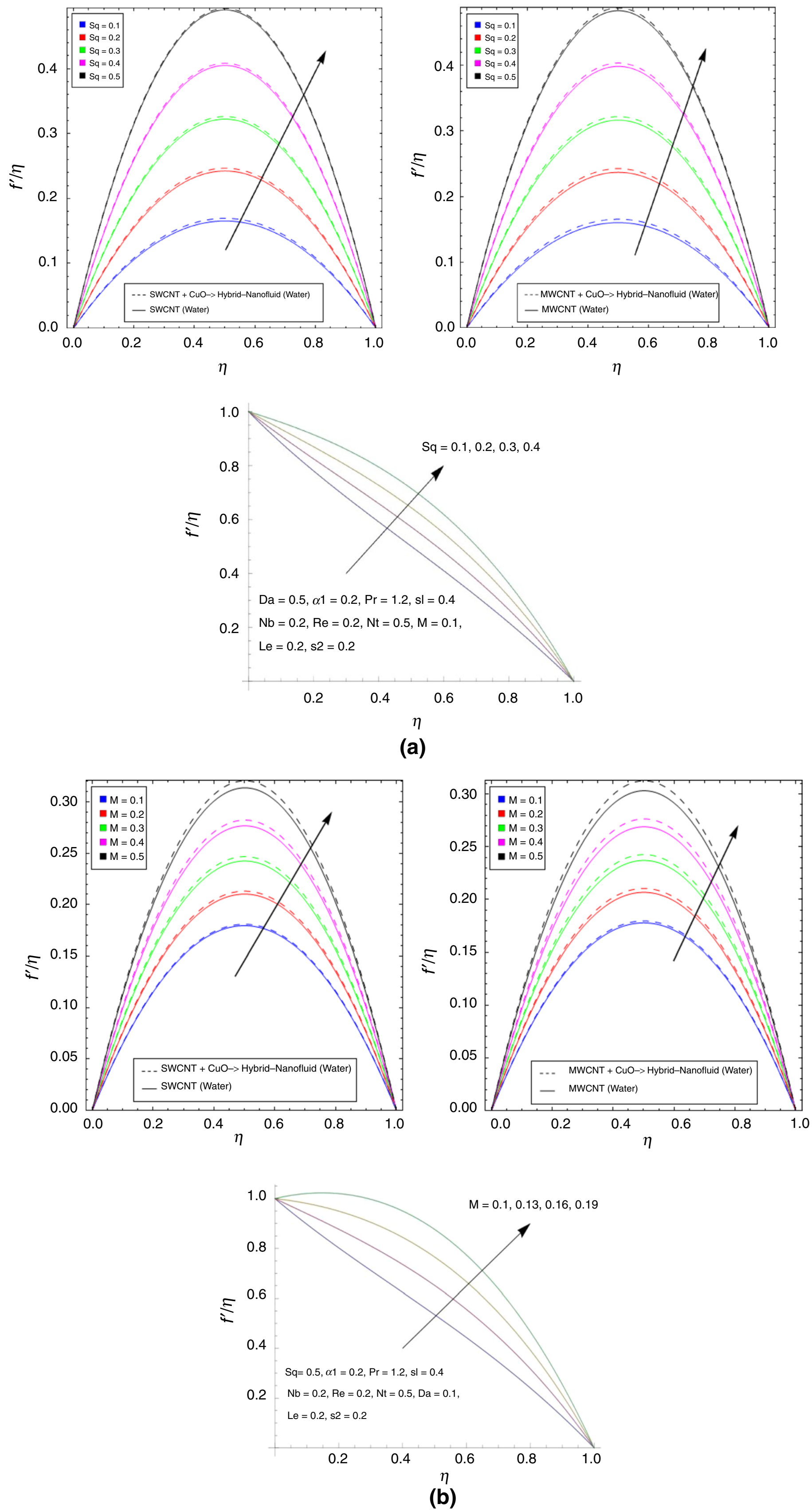

Fig. 5 **a** Comparison of current analysis and published work [35] during impact of Sq on $f'(\eta)$. **b** Comparison of current analysis and published work [35] during impact of M on $f'(\eta)$. **c** Comparison of current analysis and published work [35] during impact of Sq on $\theta(\eta)$. **d** Comparison of current analysis and published work [35] during impact of M on $\theta(\eta)$

Fig. 5 (continued)

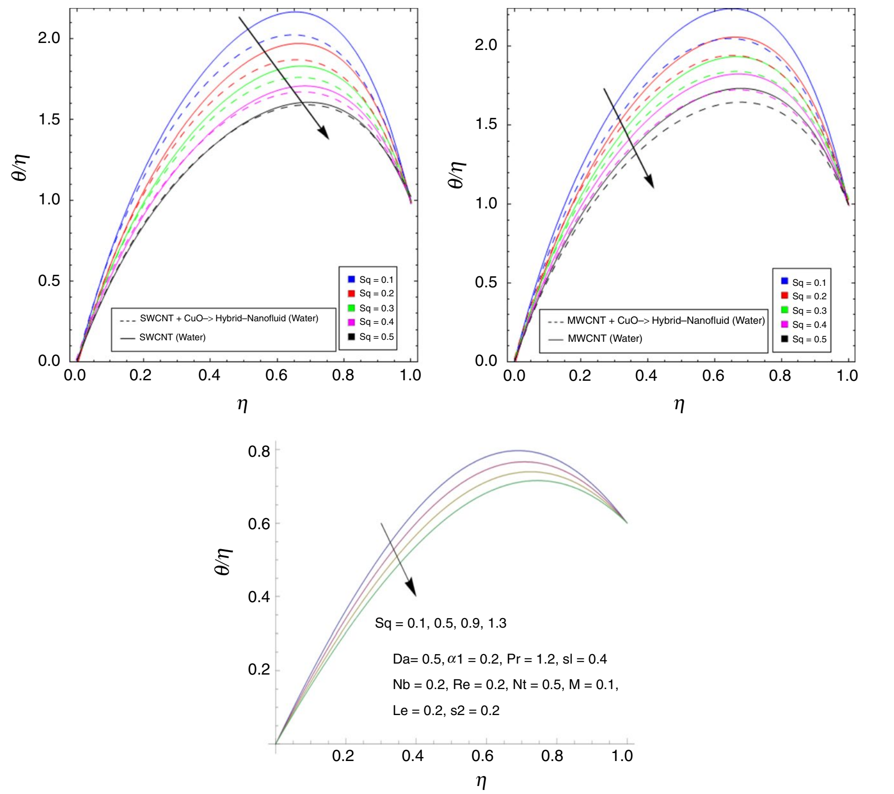

(c)

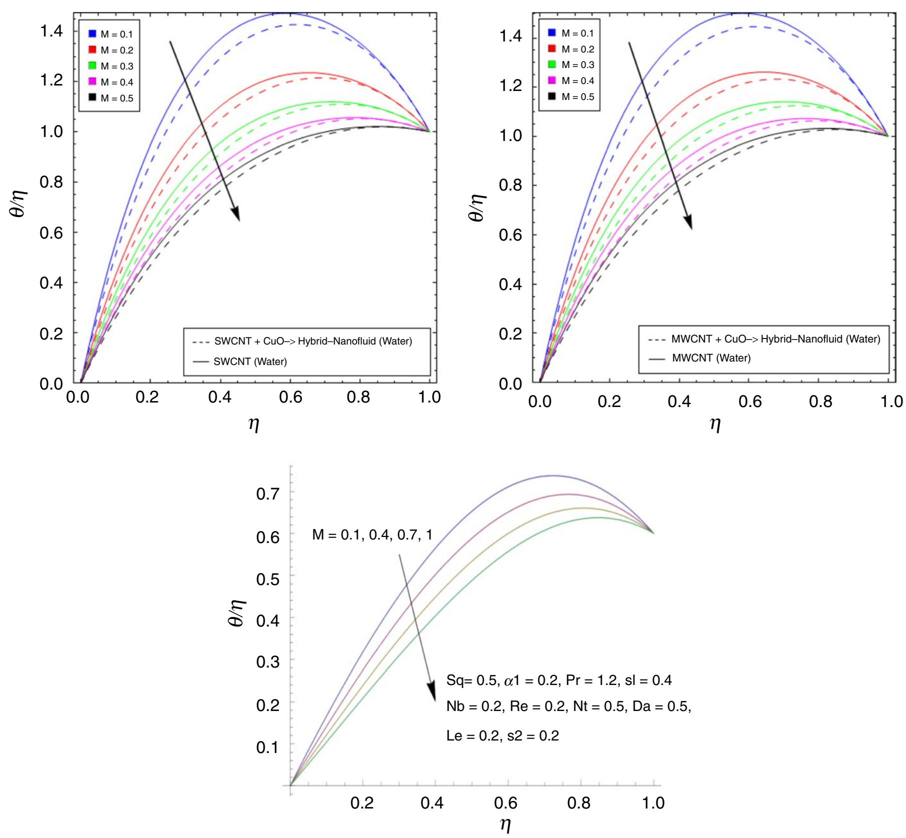

(d)

Conclusions

Velocity of fluid ($f'(\eta)$) directly varies with higher estimations of Sq ϕ_1, M and ϕ_2. As anticipated, better performance is detected for hybrid nanofluid (CNTs (SWCNTs, MWCNTs) + CuO + water) followed by nanofluid (CNTs (SWCNTs, MWCNTs + water) and basefluid (water), respectively. An increase in temperature ($\theta(\eta)$) is seen for larger Ec while it reduces with higher estimations of Sq ϕ_1, M and ϕ_2. Increment in Sq, ϕ_1, M and ϕ_2 leads to rise in Nusselt number ($\mathrm{Nu}_x (Re_x)^{-\frac{1}{2}}$). Entropy production rate (Ns) intensifies with larger of Sq M and Ec. An increment in Bejan number (Be) is detected with rise of Sq and Ec while it reduces through higher M. Impacts of hybrid nanofluid (CNTs (SWCNTs, MWCNTs + CuO + water) are more effective when compared with nanofluid (CNTs (SWCNTs, MWCNTs + water) and basefluid (water).

References

1. Choi SUS, Eastman JA (1995) Enhancing thermal conductivity of fluids with nanoparticles. In: The proceedings of the 1995 ASME international mechanical engineering congress and exposition, San Francisco, USA, ASME, FED 231/MD, vol 66, pp 99–105.
2. Hayat T, Muhammad K, Muhammad T, Alsaedi A. Melting heat in radiative flow of carbon nanotubes with homogeneous-heterogeneous reactions. Commun Theror Phys. 2018;69:441–8.
3. Hosseini SR, Ghasemian M, Sheikholeslami M, Shafee A, Li Z. Entropy analysis of nanofluid convection in a heated porous microchannel under MHD field considering solid heat generation. Powder Technol. 2019;344:914–25.
4. Hayat T, Muhammad K, Alsaedi A, Asghar S. Numerical study for melting heat transfer and homogeneous-heterogeneous reactions in flow involving carbon nanotubes. Results Phys. 2018;8:415–21.
5. Khan MI, Kumar A, Hayat T, Waqas M, Singh R. Entropy generation in flow of Carreau nanofluid. J Mol Liq. 2019;278:677–87.
6. Dinarvand S, Pop I. Free-convective flow of copper/water nanofluid about a rotating down-pointing cone using Tiwari-Das nanofluid scheme. Adv Powder Technol. 2017;28:900–9.
7. Hayat T, Ahmed B, Abbasi FM, Alsaedi A. Hydromagnetic peristalsis of water based nanofluids with temperature dependent viscosity: a comparative study. J Mol Liq. 2017;234:324–9.
8. Muhammad K, Hayat T, Alsaedi A. Squeezed flow of Jeffrey nanomaterial with convective heat and mass conditions. Phys Scr. 2019. https://doi.org/10.1088/1402-4896/ab234f.
9. Mahian O, Kolsi L, Amani M, Estellé P, Ahmadi G, Kleinstreuer C, Marshall JS, Siavashi M, Taylor RA, Niazmand H, Wongwises S, Hayat T, Kolanjiyil A, Kasaeian A, Pop I. Recent advances in modeling and simulation of nanofluid flows-Part I: fundamentals and theory. Phys Rep. 2018. https://doi.org/10.1016/j.physrep.2018.11.004.
10. Hayat T, Muhammad K, Farooq M, Alsaedi A. Melting heat transfer in stagnation point flow of carbon nanotubes towards variable thickness surface. AIP Adv. 2016;6:015214.
11. Bahiraei M, Heshmatian S. Electronics cooling with nanofluids: a critical review. Energy Convers Manag. 2018;172:438–56.
12. Alsaadi FE, Muhammad K, Hayat T, Alsaedi A, Asghar S. Numerical study of melting effect with entropy generation minimization in flow of carbon nanotubes. Journal of Thermal Analysis and Calorimetery. 2019. https://doi.org/10.1007/s10973-019-08720-9.
13. Chamkha AJ, Molana M, Rahnama A, Ghadami F. On the nanofluids applications in microchannels: a comprehensive review. Powder Technol. 2018;332:287–322.
14. Hayat T, Muhammad K, Alsaedi A, Farooq M. Features of Darcy-Forchheimer flow of carbon nanofluid in frame of chemical species with numerical significance. J. Cent. South Univ. 2019;26:1260–70.
15. Molana M. On the nanofluids application in the automotive radiator to reach the enhanced thermal performance: a review. American Journal of Heat and Mass Transfer. 2017;4:168–87.
16. Mahian O, Kianifar A, Kalogirou SA, Pop I, Wongwises S. A review of the applications of nanofluids in solar energy. Int J Heat Mass Transf. 2013;57:582–94.
17. Khan MI, Muhammad K, Hayat T, Farooq S, Alsaedi A. Numerical treatment for Darcy-Forchheimer flow of carbon nanotubes due to convectively heat nonlinear curved stretching surface. Int J Numer Meth Heat Fluid Flow. 2019. https://doi.org/10.1108/hff-01-2019-0016.
18. Kasaeian A, Daneshazarian R, Mahian O, Kolsi L, Chamkha AJ. Nanofluid flow and heat transfer in porous media: a review of the latest developments. Int J Heat Mass Transf. 2017;107:778–91.
19. Molana M. A comprehensive review on the nanofluids application in the tubular heat exchangers. Am J Heat Mass Transf. 2016;3:352–81.
20. Sarkar J, Ghosh P, Adil A. A review on hybrid nanofluids: recent research, development and applications. Renew Sustain Energy Rev. 2015;43:164–77.
21. Sajid MU, Ali HM. Thermal conductivity of hybrid nanofluids: a critical review. Int J Heat Mass Transf. 2018;126:211–34.
22. Huminic G, Huminic A. The influence of hybrid nanofluids on the performances of elliptical tube: recent research and numerical study. Int J Heat Mass Transf. 2019;129:132–43.
23. Hayat T, Nadeem S. Heat transfer enhancement with Ag-CuO/water hybrid nanofluid. Results in Physics. 2017;7:2317–24.
24. Sun B, Zhang Y, Yang D, Li H. Experimental study on heat transfer characteristics of hybrid nanofluid impinging jets. Appl Therm Eng. 2019;151:556–66.
25. Muhammad K, Hayat T, Alsaedi A, Asghar S. Stagnation point flow of basefluid (gasoline oil), nanomaterial (CNTs) and hybrid nanomaterial (CNTs + CuO): a comparative study. Material Research Express. 2019. https://doi.org/10.1088/2053-1591/ab356e.
26. Stefan MJ. Versuch ber die scheinbare adhesion. Akad Wissensch Wien Math Natur. 1874;69:713.
27. Hayat T, Muhammad K, Ullah I, Alsaedi A, Asghar S. Rotating squeezed flow with carbon nanotubes and melting heat. Phys Scr. 2018. https://doi.org/10.1088/1402-4896/aaef66.
28. Singeetham PK, Puttanna VK. Viscoplastic fluids in 2D plane squeeze flow: a matched asymptotics analysis. J Nonnewton Fluid Mech. 2019;263:154–75.
29. Ahmad S, Farooq M, Javed M, Anjum A. Slip analysis of squeezing flow using doubly stratified fluid. Results Phys. 2018;9:527–33.
30. Hayat T, Muhammad K, Farooq M, Alsaedi A. Unsteady squeezing flow of carbon nanotubes with convective boundary conditions. PLoS ONE. 2016;11:0152923.
31. Sobamowo MG, Akinshilo AT. On the analysis of squeezing flow of nanofluid between two parallel plates under the influence of magnetic field. Alex Eng J. 2018;57:1413–23.
32. Hayat T, Muhammad K, Farooq M, Alsaedi A. Squeezed flow subject to Cattaneo–Christov heat flux and rotating frame. J Mol Liq. 2016;220:216–22.

33. Sobamowo MG, Jayesimi LO, Waheed MA. Magnetohydrodynamic squeezing flow analysis of nanofluid under the effect of slip boundary conditions using variation of parameter method. Karbala Int J Mod Sci. 2018;4:107–18.
34. Hayat T, Muhammad K, Alsaedi A, Asghar S. Thermodynamics by melting in flow of an Oldroyd-B material. J Braz Soc Mech Sci Eng. 2018;40:530. https://doi.org/10.1007/s40430-018-1447-3.
35. Farooq M, Ahmad S, Javed M, Anjum A. Melting heat transfer in squeezed nanofluid flow through Darcy Forchheimer medium. ASME J Heat Transf. 2018;10(1115/1):4041497.